Remote Sensing of Environment 113 (2009) 2103–2117

Contents lists available at ScienceDirect

Remote Sensing of Environment

journal homepage: www.elsevier.com/locate/rse

Testing a MODIS Global Disturbance Index across North America

David J. Mildrexler *, Maosheng Zhao *, Steven W. Running

Numerical Terradynamic Simulation Group, Dept. of Ecosystem and Conservation Sciences, University of Montana, Missoula, MT, 59812, USA

ARTICLE INFO

Article history:
Received 23 September 2008
Received in revised form 19 May 2009
Accepted 22 May 2009

Keywords:
Ecosystem disturbance
Aqua/MODIS Land Surface Temperature (LST)
Enhanced Vegetation Index (EVI)
Range of natural variability
Wildfire
Hurricane

ABSTRACT

Large-scale ecosystem disturbances (LSEDs) have major impacts on the global carbon cycle as large pulses of CO_2 and other trace gases from terrestrial biomass loss are emitted to the atmosphere during disturbance events. The high temporal and spatial variability of the atmospheric emissions combined with the lack of a proven methodology to monitor LSEDs at the global scale make the timing, location and extent of vegetation disturbance a significant uncertainty in understanding the global carbon cycle. The MODIS Global Disturbance Index (MGDI) algorithm is designed for large-scale, regular, disturbance mapping using Aqua/Moderate Resolution Imaging Spectroradiometer (MODIS) Land Surface Temperature (LST) and Aqua/MODIS Enhanced Vegetation Index (EVI) data. The MGDI uses annual maximum composite LST data to detect fundamental changes in land-surface energy partitioning, while avoiding the high natural variability associated with tracking LST at daily, weekly, or seasonal time frames. Here we apply the full Aqua/MODIS dataset through 2006 to the improved MGDI algorithm across the woody ecosystems of North America and test the algorithm by comparison with confirmed, historical wildfire events and the windfall areas of documented major hurricanes. The MGDI accurately detects the location and extent of wildfire throughout North America and detects high and moderate severity impacts in the windfall area of major hurricanes. We also find detections associated with clear-cut logging and land-clearing on the forest–agricultural interface. The MGDI indicates that 1.5% (195,580 km^2) of the woody ecosystems within North America was disturbed in 2005 and 0.5% (67,451 km^2) was disturbed in 2006. The interannual variability is supported by wildfire detections and official burned area statistics.

1. Introduction

Large-scale ecosystem disturbances (LSEDs) such as wildfires, hurricanes, insect outbreaks, wind and ice storms, heatwaves and land use occur at varying intervals in most ecosystems worldwide. The effects of disturbances are controlled in large part by their severity, duration, frequency, timing, and spatial impacts (the size and shape of the area affected) (Picket et al., 1987; Picket & White, 1985; Reice, 1994; Sousa, 1984; Turner et al., 1997). The high temporal and spatial variability of LSEDs and the atmospheric emissions from the loss of terrestrial biomass are presently a major uncertainty in understanding the global carbon cycle (Amiro et al., 2001; Canadell et al., 2000; Fraser et al., 2000; Kurz et al., 2008; Running, 2006; van der Werf et al., 2004). At local to regional scales, atmospheric emissions triggered by LSEDs have been well documented. Results indicate that individual events (e.g. hurricanes) can trigger carbon emissions that rival carbon sequestration at continental scales (Chambers et al., 2007) while annual CO_2 emissions from wildfire in western states such as Idaho and Alaska equal or exceed the statewide emissions from fossil fuel combustion (Wiedinmyer & Neff, 2007). What is needed now is a consistent methodology that can be generalized globally to provide detailed knowledge about the effects of major disturbance on woody ecosystems.

LSEDs are poorly represented, if represented at all in global models of the biosphere–atmosphere system and may initiate unforeseen feedbacks (Bonan, 2008; Running, 2008). Climate change can alter ecological disturbance regimes raising the potential that ecosystems could switch from atmospheric carbon sinks, to sources under increased warming scenarios (Baker, 1995; Dale et al., 2001; Flannigan et al., 2000; Kurz et al., 2008; Running, 2008; Stocks et al., 1998). In the western United States increased spring temperatures and an earlier spring snowmelt have resulted in an increased frequency of large wildfire activity (Westerling et al., 2006). The increase in intensity of hurricanes in the North Atlantic over the past 30 years is highly correlated with increases in tropical sea surface temperature (Emanuel, 2005). Greater storm intensity causes elevated forest tree mortality, resulting in higher ecosystem respiration and the potential for a positive feedback with elevated atmospheric CO_2 (Chambers et al., 2007). Accurate satellite-based continental-scale information on the location, spatial extent and severity of LSEDs is a prerequisite for precise estimates of carbon emissions and the implementation of policies to reduce emissions (DeFries et al., 2007; Wiedinmyer & Neff, 2007).

* Corresponding authors. Mildrexler is to be contacted at tel.: +1 541 432 0748; fax: +1 406 243 4510. Zhao, tel.: +1 406 243 6228; fax: +1 406 243 4510.
E-mail addresses: drexler@ntsg.umt.edu (D.J. Mildrexler), zhao@ntsg.umt.edu (M. Zhao).

0034-4257/$ – see front matter © 2009 Elsevier Inc. All rights reserved.
doi:10.1016/j.rse.2009.05.016

In addition to reducing uncertainties in global carbon budgets, a proven methodology to monitor and understand LSEDs is important for evaluating various ecosystem impacts. LSEDs are a key agent of land cover change. Land cover plays an important role in various processes related to global climate and terrestrial biogeochemistry such as surface energy fluxes manifested as changes in radiometric surface temperature (Nemani et al., 1996). LSEDs alter the successional stage of vegetation having important consequences for ecosystem processes and biodiversity patterns across large scales. Accurate spatial information on disturbance location and extent has been proposed as one of the four key indicators of diversity that can be derived from Earth observation data for large area biodiversity monitoring (Duro et al., 2007). We describe an improved version of a previously developed ecosystem disturbance detection algorithm with the objective of providing a global, automated and reliable measure of ecosystem disturbance throughout woody ecosystems every year.

2. Plant canopy structure, water constraints and disturbance

A specific environments' canopy density (e.g. leaf area index) is a function of the site water balance and as water availability increases, plant canopy density increases (Grier & Running, 1977). In the absence of disturbance, vegetation will achieve maximum coverage for a specific environment. Natural fluctuations in the water balance manifest physiologically as interannual variability in the plant communities leaf area index (LAI) and must be separated from true ecological disturbance. The magnitude of the interannual variability is the largest in annual herbaceous ecosystems such as grasslands because they are shallow rooted and respond rapidly to precipitation anomalies (Knapp & Smith, 2001) and smallest in densely vegetated forests that can access water through deep root systems and continue transpiring even during dry conditions (Mildrexler et al., 2006). Therefore distinguishing disturbance events from natural variations in vegetation greenness is more difficult in annual herbaceous ecosystems than in woody ecosystems.

We define disturbance as any factor that brings about a significant change in the ecosystem LAI for a period of more than one year (Waring & Running, 2007). Areas characterized by woody vegetation have sufficient water and infrequent enough disturbance to develop and maintain relatively complex, dense, long-lived canopies. In woody ecosystems LSEDs result in a sustained disruption of ecosystem structure and function (Picket & White, 1985; Tilman, 1985) that can be detected by remote sensing for the purpose of mapping disturbance location and extent.

3. The coupling of Land Surface Temperature and Vegetation Indices for disturbance detection

Radiometric Land Surface Temperature (LST) is one of the key parameters in the physics of land-surface processes on regional and global scales, combining surface–atmosphere interactions and the energy fluxes between the atmosphere and the land surface (Mannstein, 1987; Sellers et al., 1988). Early applications of satellite-derived radiometric LST were used for relating evapotranspiration and soil moisture to surface temperature from a bare surface (Carlson et al., 1981; Sequin & Itier, 1983; Gurney & Camillo, 1984). Goward et al. (1985) suggested using the rate of change in surface temperature with the amount of vegetation to describe surface characteristics. The underlying principle for such a technique is that surface temperature decreases with an increase in vegetation density through latent heat transfer (Nemani & Running, 1989). Satellite-derived LST was used in association with remotely sensed spectral Vegetation Indices (VIs) such as the Normalized Difference Vegetation Index (NDVI) as a measure of energy balance Bowen ratios to evaluate land-surface resistance and evapotranspiration (Goward & Hope, 1989; Nemani et al., 1993; Nemani & Running, 1989). These and subsequent studies observed a strong negative relation between NDVI and LST and attributed the negative correlation to changes in vegetation cover and soil moisture (Friedl & Davis, 1994; Goetz, 1997; Nemani & Running, 1997; Price, 1990; Smith & Choudhury, 1991; Wan et al., 2004).

Many previous efforts to remotely detect LSEDs have utilized some VI or a derivative thereof, such as Fraction of Photosyntheticaly Active Radiation (FPAR) (Lambin & Strahler, 1994; Nelson & Holben, 1986; Potter et al., 2007, 2005, 2003). This approach is based on the observation that the leafy vegetation component of terrestrial ecosystems is the most fragile and therefore the most vulnerable biotic component of terrestrial ecosystems to detectable alteration during disturbance events (Potter et al., 2003). The coupling of LST and NDVI was found to substantially improve land cover characterization at regional and continental scales (Lambin & Ehrlich, 1995; Nemani & Running, 1997; Roy et al., 1997). As a metric for land cover change detection, LST/NDVI ratio metrics were statistically better at detecting changes than the NDVI metric alone, confirming the importance of LST data as a complementary source of information to NDVI data (Borak et al., 2000; Lambin & Ehrlich, 1996). Lambin and Ehrlich (1996) concluded that the two variables in the LST/NDVI ratio respond to different biophysical processes, thereby enriching the information content of indices over those represented by classic VIs. Coupling measurements on the energy exchange consequence and the vegetation density changes resulting from disturbances is a more robust approach to remotely sensing the biophysical impacts of LSEDs at continental scales than using these metrics independently.

A computationally efficient, automated algorithm developed for global scale systematic disturbance detection that utilizes the strengths of the Aqua/MODIS LST data in combination with the MODIS EVI data was described and tested over the western U.S. (Mildrexler et al., 2007). Results indicated that the MODIS Global Disturbance Index (MGDI) is effective at detecting the location and spatial extent of wildfire and is sensitive to incremental processes such as recovery of disturbed landscapes. However, the analysis was based on only two years of data, an insufficient number of years to capture the range of natural variability based on the radiometric multi-year mean of each pixel. To compensate for this short dataset, we used one standard deviation from the mean MGDI value of the entire study area as the range of natural variability. While this approach was spatially consistent, it did not recognize that land covers have unique ranges of natural variability and thereby contributed to scattered false alarms. We now test the approach of computing the range of natural variability based on the radiometric multi-year mean value of each individual pixel over 5 years of data with the aim of improving the separation of verified disturbance from natural fluctuations.

Based on the 2002–2006 Collection 4 Aqua/MODIS data, we apply the MGDI computation to the North American continent and study a diverse set of ecosystem disturbances including wildfires, hurricanes, and deforestation. Our objectives are to determine the ability of the MGDI to accurately detect the location and spatial extent of major ecosystem disturbance across the woody ecosystems of North America during 2005 and 2006 and to compute the total disturbed fraction of the woody ecosystems impacted by LSED.

4. Methods

4.1. MODIS Global Disturbance Index algorithm improvements

Disturbance by definition is an event that occurs outside the range of natural variability making it critical to clearly distinguish disturbance from the backdrop of natural variability in the development of a disturbance index. Disturbance processes vary in their rate of departure from the range of natural variability indicating the need for a multi-pronged approach to disturbance detection (Goward et al., 2008). Instantaneous disturbances, such as wildfire, result in an immediate departure of the LST/EVI ratio from the range of natural

variability, whereas non-instantaneous disturbance events, such as hurricane, depart from the range of natural variability the year after the disturbance occurs, or in the case of insect epidemics, depart incrementally over the length of the epidemic. The difference between the immediate response of instantaneous disturbances and the delayed response of non-instantaneous disturbances is controlled by the rate of disturbance and/or the hydration of the ecosystem during the disturbance event. Disturbance with a fast rate that occurs during dry periods, such as wildfire, will result in an immediate spike in the maximum LST when the vegetation is removed and a larger proportion of incoming solar energy is transferred to sensible heat flux. Disturbance that occurs during the wet season or is accompanied by significant precipitation, such as with hurricanes, will not result in an immediate increase in the maximum LST because there is abundant moisture available for evaporation to offset the loss of transpiration. However, as the ecosystem dries down the following year, the progressive mortality and severe structural damage to vegetation and the commensurate reduction in transpiration will then result in an increase in the annual maximum LST.

Because our aim is to develop a disturbance detection algorithm logic that can be generalized globally we use the annual maximum composite LST data for the MGDI. By tracking the multi-year annual maximum composite LST, we focus on the LST under driest conditions when the relationship between NDVI and LST is strongest (Goward et al., 1985; Nemani et al., 1993; Smith & Choudhury, 1991). This approach is based on the observation that midday radiometric LST is strongly related to vegetation density and therefore, is likely the single most vulnerable abiotic component of terrestrial ecosystems to detectable alteration during disturbance events. Therefore, we use LST from the Aqua/Moderate Resolution Imaging Spectroradiometer (MODIS) sensor to take advantage of Aqua's afternoon overpass time of approximately 1:30 pm. Measurements close to the peak of diurnal fluctuation better reflect the thermal response of rising leaf temperatures due to decreased latent heat flux as stomata close, and soil litter surfaces dry, accentuating differences in LST among vegetation covers (Mildrexler et al., 2007). We use EVI because saturation levels are avoided whereas NDVI tends to approach saturation level in high biomass regions, having important consequences for change detection (Huete et al., 2002). To be consistent, EVI from the Aqua sensor is used.

The instantaneous variant of the MGDI algorithm has undergone a subtle yet critical change concerning the EVI data since its inception and application to the western U.S. (Mildrexler et al., 2007). We now extract the maximum EVI post-annual maximum LST, such that

$$\mathrm{MGDI}_{\mathrm{Inst.}} = \frac{\left(\mathrm{LST}_{\max} / \mathrm{EVI}_{\max\ \mathrm{post}}\right)\mathrm{current\ year}(y)}{\left(\mathrm{LST}_{\max} / \mathrm{EVI}_{\max\ \mathrm{post}}\right)\mathrm{multi-year\ mean}(y-1)} \quad (1)$$

where $\mathrm{MGDI}_{\mathrm{Inst.}}$ is the instantaneous MGDI value, $\mathrm{LST}_{\max}$ is the annual maximum 8-day composite LST in °C, $\mathrm{EVI}_{\max\ \mathrm{post}}$ is the maximum 16-day EVI following the $\mathrm{LST}_{\max}$, current year (y) is the year being evaluated for disturbance and multi-year mean $(y-1)$ is the mean of the ratios excluding the current year. The instantaneous algorithm is used for continuous wall-to-wall disturbance detection.

The non-instantaneous variant of the MGDI algorithm uses annual maximum composite LST and EVI data such that

$$\mathrm{MGDI}_{\mathrm{Non-Inst.}} = \frac{(\mathrm{LST}_{\max} / \mathrm{EVI}_{\max})\mathrm{current\ year}(y)}{(\mathrm{LST}_{\max} / \mathrm{EVI}_{\max})\mathrm{multi-year\ mean}(y-1)} \quad (2)$$

where $\mathrm{DI}_{\mathrm{Non\text{-}Inst.}}$ is the non-instantaneous MGDI value, $\mathrm{LST}_{\max}$ is the annual maximum 8-day composite LST in °C, $\mathrm{EVI}_{\max}$ is the annual maximum 16-day composite EVI, current year (y) is the year being evaluated for disturbance and multi-year mean $(y-1)$ is the mean of the ratios excluding the current year. The non-instantaneous algorithm is used to specifically focus on the windfall impacts of historical hurricanes and is not used for wall-to-wall disturbance detection.

The logic behind the MGDI equations is illustrated in the conceptual models (Fig. 1). The MGDI is a dimensionless value and in the absence of disturbance, a given pixel's MGDI value will tend toward unity (e.g. multi-year mean equals 1.0). However, the energy balance of a land area is not static and will fluctuate within a range of natural variability during both dry and wet years (in green). When a major disturbance event, such as wildfire occurs, LST will increase and EVI will decrease instantaneously, resulting in a MGDI value that is much larger than the multi-year mean (Fig. 1a). The disturbance event (in red) is detected as it moves outside the range of natural variability. As the area recovers from disturbance as defined by increasing EVI and decreasing LST, the bi-directional nature of the MGDI will track the incremental change toward recovery and the zone of natural variability. The conceptual diagram is similar for large hurricanes (i.e. non-instantaneous disturbance) except that the LST/EVI signal will be much larger than the multi-year mean the year following disturbance due to the hydration of the land surface during the hurricane and progressive delayed mortality of damaged vegetation (Fig. 1b). This study focuses on negative disturbances that result in a reduction in the leaf area and an increase in the LST.

5. Algorithm processing chain

5.1. Step 1: annual maximum compositing of Aqua/MODIS LST data

Apply annual maximum value compositing to the LST data, selecting independently for each pixel the maximum 8-day LST over a one-year period from all 8-day composites labeled as reliable by the

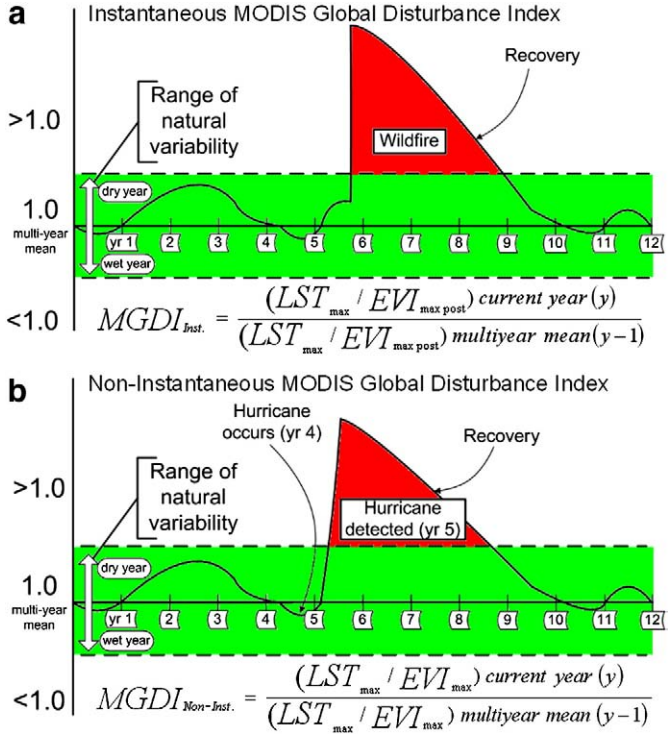

Fig. 1. The MGDI algorithm and conceptual models illustrating the energy balance of a given land area through time. In the absence of disturbance, the MGDI values approach unity (e.g. multi-year mean equals 1.0) and exist within a range of natural variability defined by fluctuations between wet and dry years (green zone). Disturbance causes changes in the $\mathrm{LST}_{\max}$, $\mathrm{EVI}_{\max}$ or $\mathrm{EVI}_{\max\ \mathrm{post}}$ values. In the case of wildfire (a, instantaneous disturbance), the $\mathrm{LST}_{\max}$ increases and the $\mathrm{EVI}_{\max\ \mathrm{post}}$ decreases resulting in a larger current year ratio relative to the multi-year mean and a divergence from the range of natural variability (in red). Hurricanes hydrate the land surface dampening an immediate spike in LST and prolonging the die-back of damaged vegetation (b, non-instantaneous disturbance). Therefore the MGDI value will increase the year after the disturbance event (in red).

quality control (QC). Combine the LST data into one seamless image representing the hottest LST detected at every pixel throughout an annual period. The date of the maximum LST acquisition for each pixel is also extracted and combined into one image for use in choosing the $EVI_{max\ post}$ (Step 2). Satellite-derived LST is influenced by synoptic weather variability (wind-speed, cloud cover, humidity, radiation loading, etc.) on a daily, even hourly basis, and has high natural variability (Friedl & Davis, 1994; Nemani & Running, 1997). Step 1 removes the natural synoptic variability associated with daily to seasonal LST while retaining the fundamental impact on the land-surface energy partitioning that LSEDs impart on woody ecosystems.

5.2. Step 2: EVI data processing

A baseline threshold of 0.025 representing the lower boundary condition of vegetation was established for EVI and all pixels with values less than the threshold were reclassified as no data. These values are primarily associated with water bodies and snow/ice and the basic premise that the lower baseline contains only non-photosynthetic targets (Huete et al., 1999).

5.2.1. Instantaneous disturbance

Extract the maximum EVI value that occurs after the annual maximum LST and during the same year at every pixel. This ensures that; 1) the EVI value does not precede the wildfire event while the LST_{max} follows it and, 2) a low EVI value, perhaps due to stress at the end of a long, dry summer, but not representing true disturbance, is not falsely flagged as disturbed.

5.2.2. Non-instantaneous disturbance

Apply annual maximum value compositing to the EVI data, selecting independently for each pixel the maximum 16-day EVI over a one-year period from all 16-day composites labeled as reliable by the QC.

5.3. Step 3: compute LST/EVI annual ratios

Divide the LST by the EVI on a pixel-by-pixel basis for each successive interannual period resulting in a ratio of LST_{max} to $EVI_{max\ post}$ for instantaneous disturbance and LST_{max} to EVI_{max} for non-instantaneous disturbance. This results in a unitless value that shows strong sensitivity to changes in either variable.

5.4. Step 4: compute multi-year LST/EVI ratio means

The mean of the LST/EVI ratios is computed for all years $(y-1)$ excluding the current year (y), or the year being evaluated for disturbance. The mean LST/EVI ratio reflects the undisturbed energy balance of the land surface and provides a solid baseline to assess departure from the range of natural variability. It is important to have several years of data so that the pixel mean can normalize to reflect natural variability associated with fluctuations between wet and dry years (Mildrexler et al., 2007).

5.5. Step 5: compute MGDI values

Divide the LST/EVI ratios of the year being evaluated for disturbance by the mean of the LST/EVI ratios for all previous years on a pixel-by-pixel basis. For example, the 2005 MGDI is computed as the 2005 LST/EVI ratios divided by the mean of the 2002–2004 LST/EVI ratios. The 2006 MGDI is computed as the 2006 LST/EVI ratios divided by the mean of the 2002–2005 LST/EVI ratios.

5.6. Step 6: apply threshold for disturbance detection

To determine the threshold for flagging a pixel as disturbed, we used an extensive pixel-based analysis of the impact of verified wildfire disturbance on the pre- and post-disturbance LST_{max}, $EVI_{max\ post}$ and MGDI values. Fig. 2 shows an example of this analysis where four subsets consisting of 16 pixels each were established within 2006 wildfire perimeter maps over a large latitudinal gradient in North America. We extracted the LST_{max}, $EVI_{max\ post}$, and MGDI values at each pixel during 2005 and 2006 and computed the percent change. The values for every pixel are given in Appendix A. Fig. 2b illustrates the abrupt negative change in EVI between pre- and post-fire scenes that closely corresponds with the wildfire perimeter area provided by Canadian Center for Remote Sensing (CCRS) for the Saskatchewan study area. The EVI values typically show decreases of more than 50% within the fire area. Fig. 2c illustrates the spike in LST that followed the fire in clear association with the wildfire perimeter map. LST increases between 10 °C and 30 °C are common within the wildfire boundary. Fig. 2d shows that the percent change in the MGDI values from 2005 to 2006 are much larger (>200%) than the percent change in the EVI or LST values alone. Results from these four study sites are summarized in Table 1 and indicate that across a large latitudinal gradient that encompasses a variety of woody ecosystems with different fire regimes, the wildfire signal that the MGDI tracks is consistently strong. Even low-intensity wildfire has immediate impacts on the effected area including consumed understory and blackened surfaces that are best detected instantaneously.

Because our aim is to develop a methodology that is also sensitive to non-fire disturbances, the threshold for disturbance detection should be lower than the minimum percent change of the MGDI for wildfire (98.9%, North Cascades subset, Table S1 in Appendix A). We test three disturbance thresholds, 45%, 65% and 75% increases from the multi-year mean value. Based on visual analysis of background noise and the calculation of total disturbed surface area in woody ecosystems across North America at each threshold, we selected 65% as our threshold for instantaneous disturbance and 45% as our threshold for non-instantaneous disturbance.

5.7. Step 7: apply filter to eliminate false detects

False detects due to uncertainties in the MODIS EVI and LST products introduce some background noise that shows up as spatially scattered disturbed pixels in the resultant MGDI image. Also, the conversion of the datasets from sinusoidal projection to Lambert azimuthal equal area projection using nearest neighbor resampling results in some distortion. This artifact of image re-projection was discovered to be causing chronic false positives in tessellated patterns across the study area. This distortion manifests itself as a doubling of the same pixel (Fig. 3a). An automated cleaning technique has been developed to solve these problems while making sure that pixels on the border of disturbed areas are not masked out (Fig. 3b).

We partially adopted a filter method proposed by Fraser et al. (2000) for their burned area mapping. First, each pixel flagged as disturbed is retained if at least four surrounding pixels are also disturbed within its 3×3 pixel window. Otherwise, the pixel will be masked out as a non-disturbed pixel. The side effect of this method is that it can eliminate pixels on the boundary of verified disturbance because many boundary pixels have less than four surrounding disturbed pixels. To solve this problem, if the removed boundary pixels were attached with a disturbed patch in the cleaned images, they are reflagged as disturbance. In addition to this improvement, the other major difference between our method and Fraser et al. (2000) is that we did not flag any undisturbed pixel as disturbed to smooth the final results.

6. MGDI application and testing

We applied the MGDI algorithm described above to the Aqua/MODIS data for the years 2002–2006 across North America. The dataset is composed of Aqua/MODIS 8-day composite daytime LST,

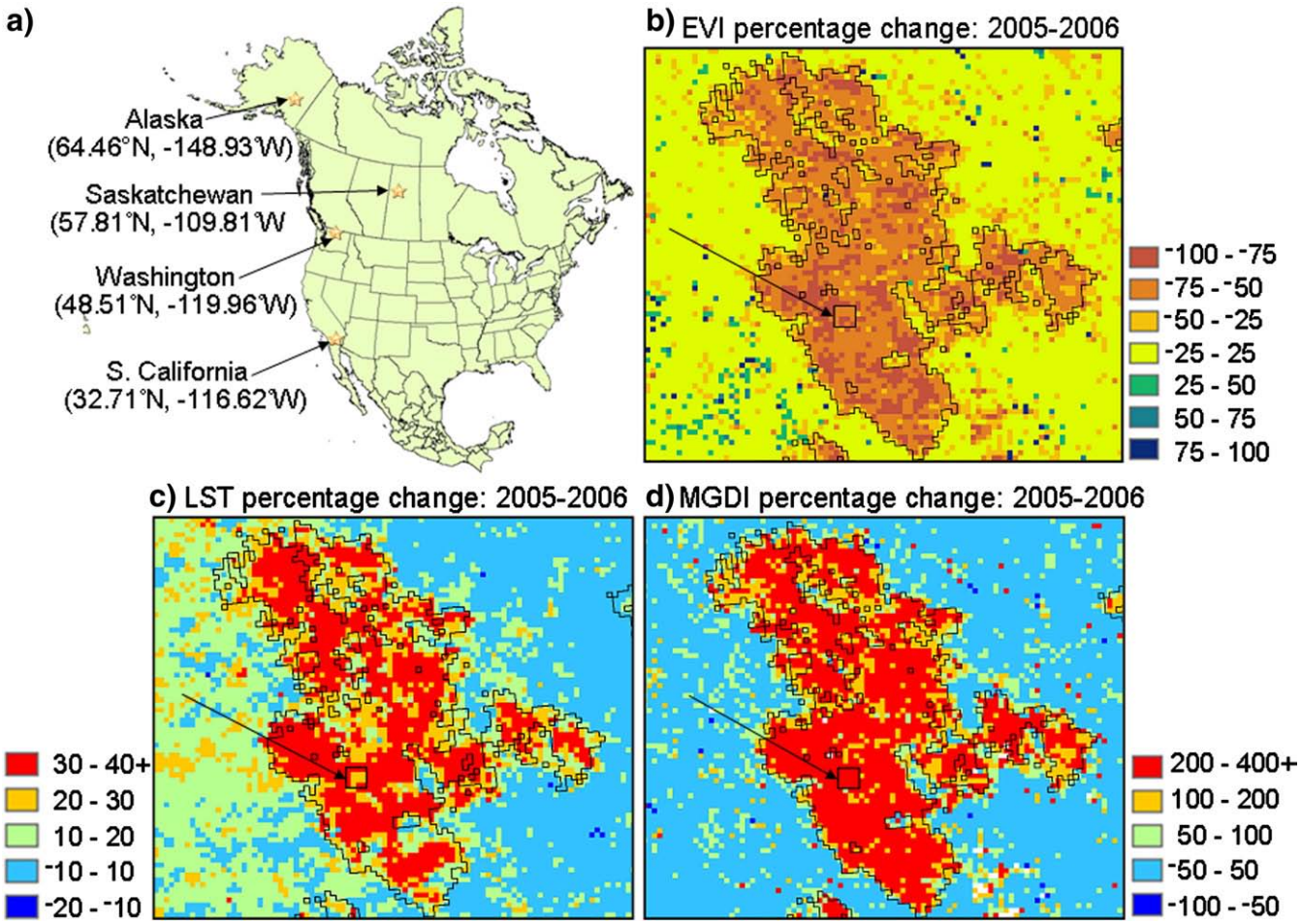

Fig. 2. Location of study sites within verified wildfire areas used for percent change analysis of LST_{max}, $EVI_{max\ post}$ and MGDI from 2005 to 2006. The Saskatchewan study site showed an average $EVI_{max\ post}$ reduction of over 70%, an LST_{max} increase of 37% and a MGDI increase of 392%. This illustrates the abrupt impact that wildfire leaves on the landscape, the benefit of combining EVI and LST together in a disturbance index, and the powerful approach of the MGDI at magnifying the disturbance signal through the LST/EVI ratioing approach.

Aqua/MODIS 16-day composite EVI, and Terra/MODIS Land Cover Type 1 (IGBP) data. All MODIS data used for this study are Collection 4 data with a spatial resolution of 1 km. MODIS QC flags were used for the LST and EVI data to remove pixels with cloud contamination. The HDF-EOS data were then converted to raster images for further analysis.

We concentrate on woody ecosystems because of the fundamental difference in ecosystem processes between woody and annual ecosystems: 1) The MGDI is designed to detect LSEDs that result in a sustained disruption of ecosystem structure and function. Disturbance in annual herbaceous ecosystems (e.g. grasslands, croplands) where a wildfire may occur in the fall, followed by rapid and complete recovery of vegetation by early summer, does not fit this definition. 2) In the U.S., the importance of the contribution of emissions of CO_2 from wildfire to the atmosphere from LSEDs is much greater from woody ecosystems than from annual herbaceous ecosystems (Wiedinmyer & Neff, 2007). 3) Annual herbaceous ecosystems such as grasslands have the capacity for large, rapid production responses to high precipitation levels (Huxman et al., 2004; Knapp & Smith, 2001; White et al., 2005). The large variability in the vegetation productivity of grasslands as measured by the EVI does not represent true ecological disturbance. Even with our algorithm improvements, the responses of grasslands to precipitation fluctuations are still problematic and are sometimes incorrectly flagged as disturbance. Potter et al. (2005) applied detection of sustained FPAR low events to 18 years of Advanced Very High Resolution Radiometer (AVHRR) data across North America and concluded that 52% of LSEDs occurred in forested ecosystems, 28% occurred in savanna and shrublands, and 20% occurred in grasslands and croplands. Based on these results approximately 80% of LSED in North America occurs within woody vegetation that we concentrate on in this study.

The MODIS land cover is used to mask out all non-woody pixels leaving all pixels classified as evergreen needleleaf forests, evergreen broadleaf forests, deciduous needleleaf forests, deciduous broadleaf forests, mixed forests, open and closed shrublands, woody savannas and savannas. While this approach is not ideal because of uncertainties in the MODIS land cover, it does provide a spatially consistent methodology for focusing our analysis on woody cover types. Based on

Table 1
The percent change in the $EVI_{max\ post}$, the annual LST_{max} and the MGDI from 2005 to 2006 for verified wildfire.

Study area	$EVI_{max\ post}$ % change	LST_{max} % change	MGDI % change
Alaska	−53	29	190
Saskatchewan	−70	37	392
Washington	−76	30	582
California	−59	25	231

The values are the mean of 16 pixels within documented wildfire perimeters established to cover a large latitudinal range (Fig. 2). Wildfire results in a large reduction in the vegetation density and a commensurate increase in the LST. The MGDI percent change is much higher than the EVI or LST alone due to the ratioing approach that magnifies the disturbance signal.

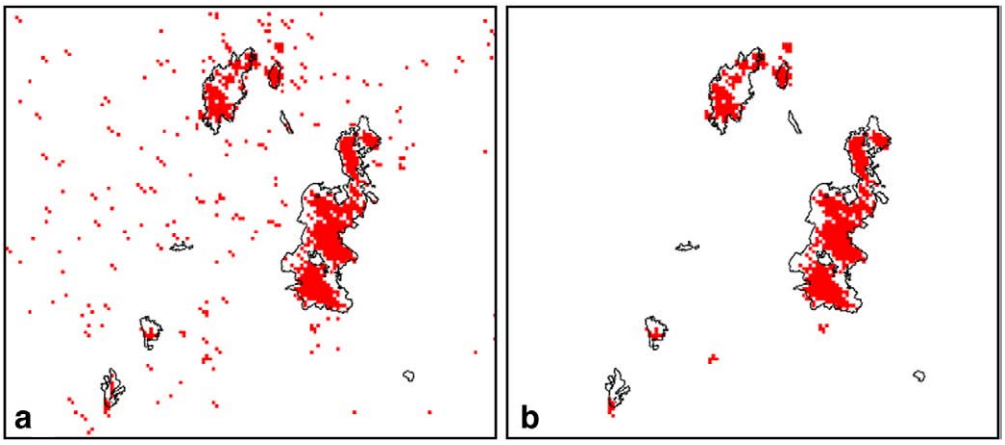

Fig. 3. Before (a) and after (b) filter application of the MGDI results for wildfire in Washington's North Cascade Mountains (corresponds to Fig. 6e). The scattered pixels flagged by the MGDI are due to uncertainties in the MODIS data and pixel distortion that results from reprojection of the datasets. The filter is designed to remove these false detections while retaining flagged pixels on the edge of large disturbances, such as wildfire areas.

this approach, 62.7% of the study domain is covered by woody vegetation. The range of natural variability is defined on a pixel specific level as the MGDI values that are no more than 65% greater than the multi-year mean for instantaneous disturbance and no more than 45% greater than the multi-year mean for non-instantaneous disturbance. These values are mapped as no color. Any pixels that have MGDI values above these thresholds are flagged as disturbance. Disturbance severity is separated into two classes, moderate and high, based on the magnitude of divergence from the multi-year mean. Disturbed pixels with values that are less than 100% greater than the multi-year mean are mapped in orange (moderate) and values that are 100% and greater than the multi-year mean are mapped in red (high). This threshold is based on the examination of the impacts of wildfire on the MGDI values described in Step 6 of the Algorithm Processing Chain above.

Verification of the MGDI results is divided into detection of wildfire, hurricane and deforestation related disturbance events. We focus on the years 2005 and 2006 as our algorithm is designed to separate disturbance and natural variability better with more years of data.

6.1. Wildfire detection

Verification of wildfire detection by the MGDI is based upon close association with independently confirmed, well-documented wildfire perimeter datasets that are developed to provide coarse-resolution burned area information across large areas. At continental scales, variation exists in the availability and attributes of wildfire perimeter map datasets. For example, to our knowledge, no such datasets are available for Mexico. Wildfire perimeter maps for the U.S. were obtained from the United States Geological Survey (USGS) and the United States Forest Service (USFS) and are derived from interpretation of infrared imagery, aerial and field-based Global Positioning System surveys, and on screen digitization. These datasets are not intended to be comprehensive (e.g. to include all wildfires for a given year) and they do not distinguish unburned islands within fire perimeters. Wildfire perimeter maps for Canada were acquired from the CCRS and based on a technique developed by Fraser et al. (2000) where burned areas are mapped by combining an annual AVHRR hotspot map with observed changes in a VI from the SPOT VGT sensor. Pixels with a significant drop in the index that are spatially coupled to an AVHRR hotspot are mapped as being burned (Fraser et al., 2000). This dataset is intended to provide comprehensive information for large burns (>10 km^2) and has been well verified. Wildfire perimeter maps provide knowledge of the spatial extent of the burned area with a high level of accuracy and permit a rigorous quantification of the algorithm performance. To quantify the performance of the MGDI algorithm for wildfire detection, we compare the results against the wildfire perimeter dataset from Fraser et al. (2000) because it is intended to be comprehensive and covers all of Canada. The GIS fire perimeters were assigned a reference number and the total number of pixels within each polygon was quantified. Then we compared the total number of pixels in each wildfire perimeter polygon to the total number of pixels detected within the associated MGDI disturbance patch. Pixels flagged as disturbed by the MDGI that are outside the HANDS fire perimeter polygons are included in the analysis as errors of commission only if they are connected to a disturbed patch that is associated with a specific HANDS fire perimeter.

In addition to comparison with GIS datasets of burn boundaries, we use total burned area datasets for portions of Canada and the U.S. to determine if the interannual variability in wildfire detected by the MGDI from 2005 to 2006 is supported by total burned area statistics. Total burned area data for Quebec were obtained from the National Forestry Database Program (NFDP) established by the Canadian Forest Service (http://nfdp.ccfm.org/fires/national_e.php). Total burned area data for Alaska was obtained through the Alaska Department of Natural Resources, Division of Forestry (http://forestry.alaska.gov/firestats/).

6.2. Hurricane detection

The 2005 Atlantic hurricane season was the most active Atlantic hurricane season in recorded history providing several opportunities to test the non-instantaneous MGDI results. Hurricanes are complex disturbance events having widespread heterogeneous effects on vegetation such as sudden and massive tree mortality and delayed mortality (Lugo, 2000; Lugo & Scatena, 1996). Dale et al. (2001) estimate that the average annual areal extent impacted by hurricanes in the U.S. at over 10,000 km^2. In general, impacts are greater where the hurricane first crosses over land. Hurricane impacts decrease as the storm moves inland and begins dissipation. We examine patterns of disturbance detection in the windfall areas of Hurricane Katrina, Hurricane Rita and Hurricane Wilma. Hurricane stormtrack images are credited to the University of Wisconsin/Cooperative Institute for Meteorological Satellite Studies (CIMSS)/Space Science and Engineering Center (SSEC). Association between the MGDI results and impacts of Hurricane Katrina on the Bayou Sauvage National Wildlife Refuge (NWR) is examined with Landsat imagery and GIS data obtained through the U.S. Fish and Wildlife Service (http://www.fws.gov/data/datafws.html).

6.3. Deforestation and logging detection

Deforestation is defined as conversion from forest land to non-forest land and includes clearing of forests for agriculture. Forest degradation practices include unsustainable timber extraction such as large-scale clear-cut logging. Deforestation and heavy commercial logging result in a severe reduction in vegetation density and a commensurate increase in LST. However, for successful detection the impacted area must be large enough to pass the filter (see Step 7 of Processing Chain). This suggests that only relatively large deforestation and clear-cut logging, exceeding several continuous kilometers will be detected. To verify if anthropogenic disturbance occurred at areas flagged by the MGDI, the latitude and longitude of the center of disturbed pixels are extracted from GIS and used to insert corresponding pointers in Google Earth. Google Earth has potential problems with geolocation and little temporal information on date of image acquisition compared to MODIS data. Therefore rather than looking for exact correspondence, our purpose is to verify if pixels flagged by the MGDI generally correspond to anthropogenic disturbance and are in areas where we would expect to see deforestation such as on the forest–agricultural interface.

6.4. Continental disturbance statistics

Continental-scale disturbance statistics are critical for understanding how much total surface area was disturbed, which cover types have the highest rates of disturbance and for assessing interannual variability in disturbance rates. Based on the results of the MGDI instantaneous approach, we compute the total disturbed area for woody ecosystems of North America and for the major biome groups (forests, shrublands, and savannas) that compose woody cover types during 2005 and 2006. The MGDI results are compared to initial disturbance estimates for the U.S. from the North American Forest Dynamics (NAFD) study (Goward et al., 2008). Combined, comparison with the GIS databases for wildfire, association with historical hurricane stormtrack images, and comparison with burned area and total disturbed area statistics permit a rigorous evaluation of the algorithm.

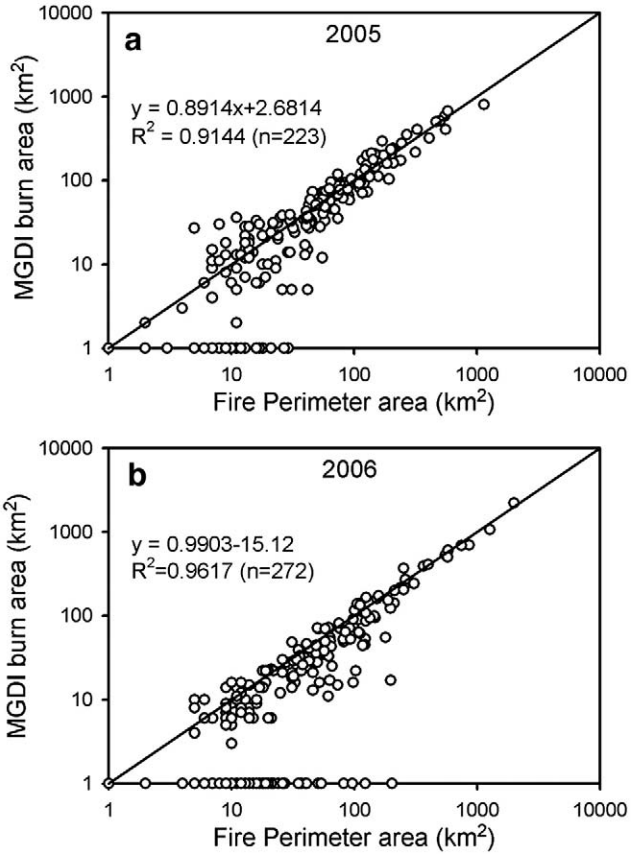

Fig. 4. The relationship between the area of the GIS fire perimeter data and the corresponding MGDI disturbance patch for 2005 and 2006 across the woody ecosystems of Canada. The datasets are compared on a logarithmic scale and with a line illustrating 1:1 agreement. Data points on the *x*-axis represent wildfire perimeters with no MGDI detections.

7. Results

7.1. Wildfire detection

The relationship between the area of each GIS wildfire perimeter map within Canada and the corresponding MGDI disturbance patch for 2005 and 2006 is given is Fig. 4. We present the data on a logarithmic scale so that the data distribution can be seen more clearly, especially the numerous smaller values. While the overall association is very close for 2005 ($R^2 = 0.91$, $p<0.001$) and 2006 ($R^2 = 0.96$, $p<0.001$), the larger burns show a stronger association than the smaller burns. This finding is consistent with Fraser et al. (2000). Burns that were missed by the MGDI or incorrectly identified by the validation dataset are shown on the *x*-axis. The average size of the missed burns is 9.4 km^2 during 2005 and 16.5 km^2 for 2006.

The 2006 continuous MGDI results for instantaneous disturbance across the woody ecosystems of North America are presented in Fig. 5. We examine in detail the association between pixels flagged by the MGDI and independently confirmed, documented wildfire events across most of the major wildfire regions of North America.

Fig. 6 shows the close-up images that correspond to each location in Fig. 5. Across the study area the MGDI results show strong spatial association with the 2006 wildfire perimeter maps (black polygons) with minor to no background noise for the Parks Highway Fire in Alaska (a), boreal forest wildfires in Saskatchewan (b), large wildfires along the border of British Columbia and Alberta (c), wildfires in Quebec (d), the Tripod and Tatoosh Fires in Washington State and British Columbia (e) the Red Eagle Fire in Montana (f), the Cascade Crest Complex Fires in Oregon (g), the Cavity Lake Fire in the Boundary Waters Wilderness of Minnesota (h), the Canyon Fire in California (i) and the Warm Fire in Arizona (j).

Exceptions include two small fire perimeters where the MGDI does not flag any pixels (Fig. 6c, circle outlines). Several pixels were confirmed as disturbed within the lower small fire perimeter (circle outline) that were subsequently lost to the filter. In the same scene the MGDI detects disturbance in only a portion of one fire perimeter (triangle outline) and flags a continuous group of pixels that correspond with four separate wildfire perimeter maps (square outline). Further examination of this scene reveals that the decrease in the 2006 $EVI_{max\ post}$ data corresponds to the MGDI detections rather than the validation data (Fig. 7). In several scenes portions of the wildfire perimeter boundaries extend beyond the MGDI detection (Fig. 6a, h, i, and j). Potential factors contributing to these discrepancies include non-woody pixels that are masked out of the MGDI analysis, patchy low-intensity fire that may have gone undetected, and fire perimeter maps that can overestimate the burned area.

The large well-defined disturbance patch detected in the center of Fig. 6d (circle outline) does not correspond with a wildfire perimeter map. The size of this disturbance patch is estimated to be over 235 km^2. This is a conservative estimate as some disturbed pixels have been masked out as non-woody land covers. Closer examination reveals that in 2006, this area had a reduction in EVI (circle outline) similar in magnitude to surrounding areas that were impacted by wildfire in 2006 (Fig. 8a, black polygons). However, the 2006 maximum LST sharply declined relative to 2005, opposite of the

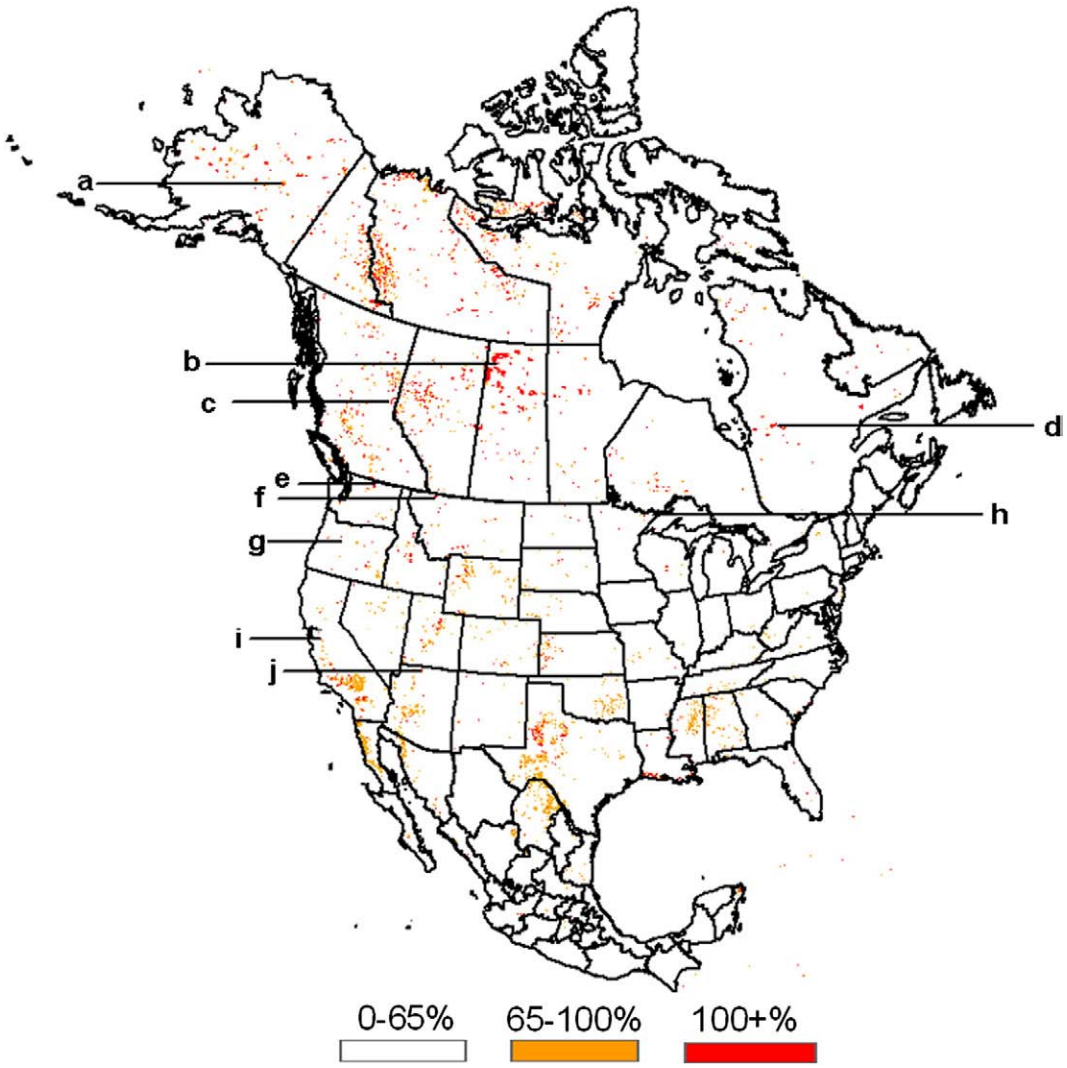

Fig. 5. The 2006 MGDI results for North America. Moderate intensity disturbance is mapped in orange and represents a 65–100% divergence of the current year MGDI value from the range of natural variability. High intensity disturbance (in red) signals a divergence of over 100%. Locations a–j correspond to close-up comparisons between the MGDI results and wildfire perimeter maps shown in Fig. 6.

areas impacted by wildfire (Fig. 8b). This magnitude of EVI change is not typical of stressed vegetation and indicates that the vegetation has died in this area. Aerial images show that this is a swampy, muskeg environment, with rivers and standing water. We surmise that this area may have flooded, killing the vegetation and greatly reducing the maximum LST.

The disturbance regime of the boreal forest is dominated by wildfire and regional images of disturbance detection by the MGDI during 2005 and 2006 illustrate high interannual variability (Fig. 9). In Alaska a large number of wildfires were detected in association with wildfire perimeter maps in 2005 (top left) and only a few in 2006 (bottom left). Burned area totals for Alaska were 18,874 km^2 for 2005, and in 2006 that number dropped dramatically to only 1078 km^2. Alaska was in a severe drought in August of 2005, which is usually one of Alaska's wettest months (Hayasaka et al., 2006). The extreme conditions in 2005 resulted in more wildfires and unusually low vegetation density measurements, especially in open shrublands. A similar trend occurred in Quebec where in 2005 the MGDI detected a large number of wildfires across the Province in close association with the GIS perimeter maps (top right) and relatively few in 2006 (bottom right). The provincial burned area statistics for Quebec report 8001 km^2 of total burned area in 2005 and 1364 km^2 for 2006.

7.2. Hurricane detection

Hurricane Katrina made landfall on August 29th, 2005 in Louisiana and continued north through Mississippi and Alabama (Fig. 10a). The 2006 non-instantaneous MGDI detects complex patterns of high and moderate severity disturbance in the area of the stormtrack (Fig. 10b). The highest severity impacts (>100%) are detected where Hurricane Katrina initially crossed over land in Louisiana. Further inland the MGDI detects a mixture of large contiguous patches and scattered moderate severity disturbance (45–100%).

A zoom-in of the Bayou Sauvage NWR (black polygon, Fig. 10c) shows that the 2006 MGDI detects a contiguous patch of high and moderate severity disturbance across a large portion of the refuge. A

Fig. 6. Correspondence between the 2006 MGDI results and 2006 wildfire perimeter maps (black polygons) for the Parks Highway fire in Alaska (a), wildfire in Saskatchewan's boreal forest region (b), a group of wildfires on the British Columbia, Alberta border (c), numerous wildfires in Quebec (d), the Tripod and Tatoosh wildfires in Washington State (e), the Red Eagle fire in Montana (f), the Cascade Crest complex in Oregon's Cascade Mountains (g), the Cavity lake Wildfire in the Boundary Water Wilderness, Minnesota (h), the Canyon Fire in California (i), and the Warm Fire in Arizona (j).

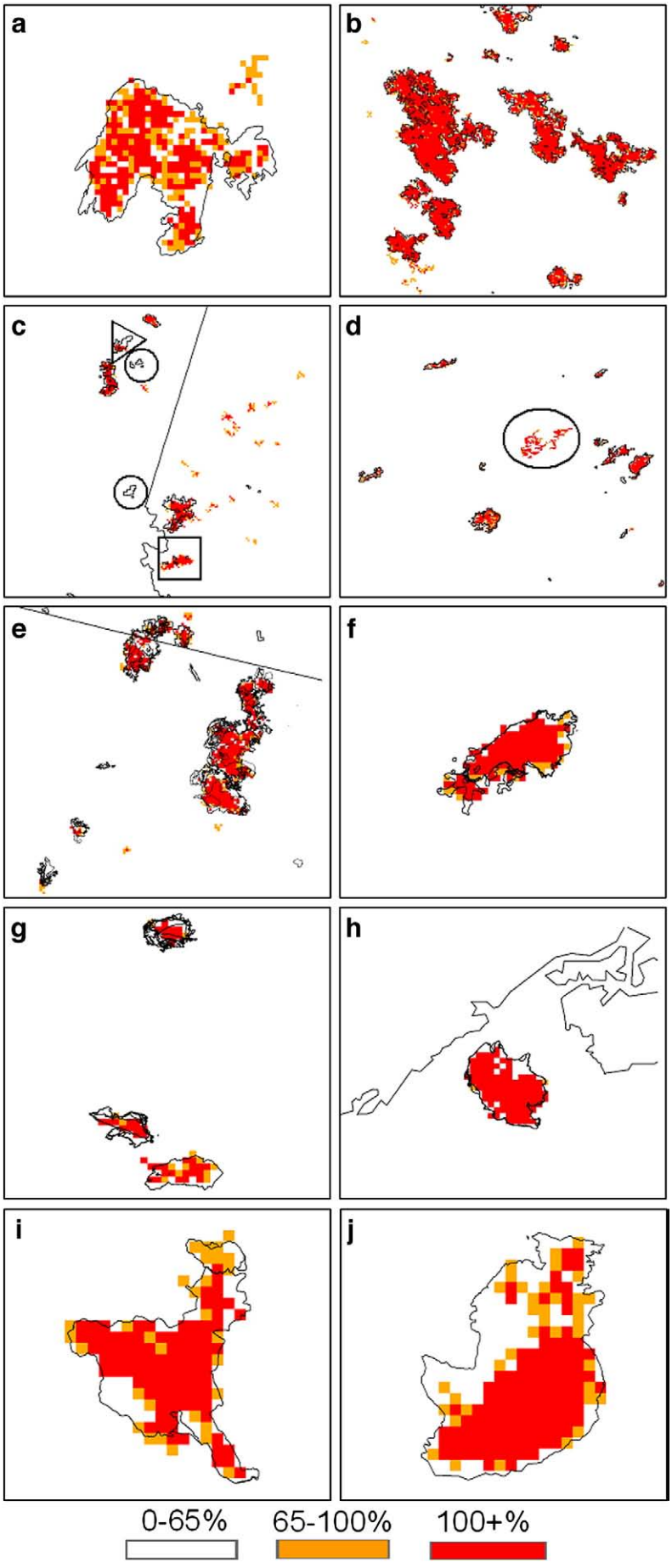
a
b
c
d
e
f
g
h
i
j
0-65%
65-100%
100+%

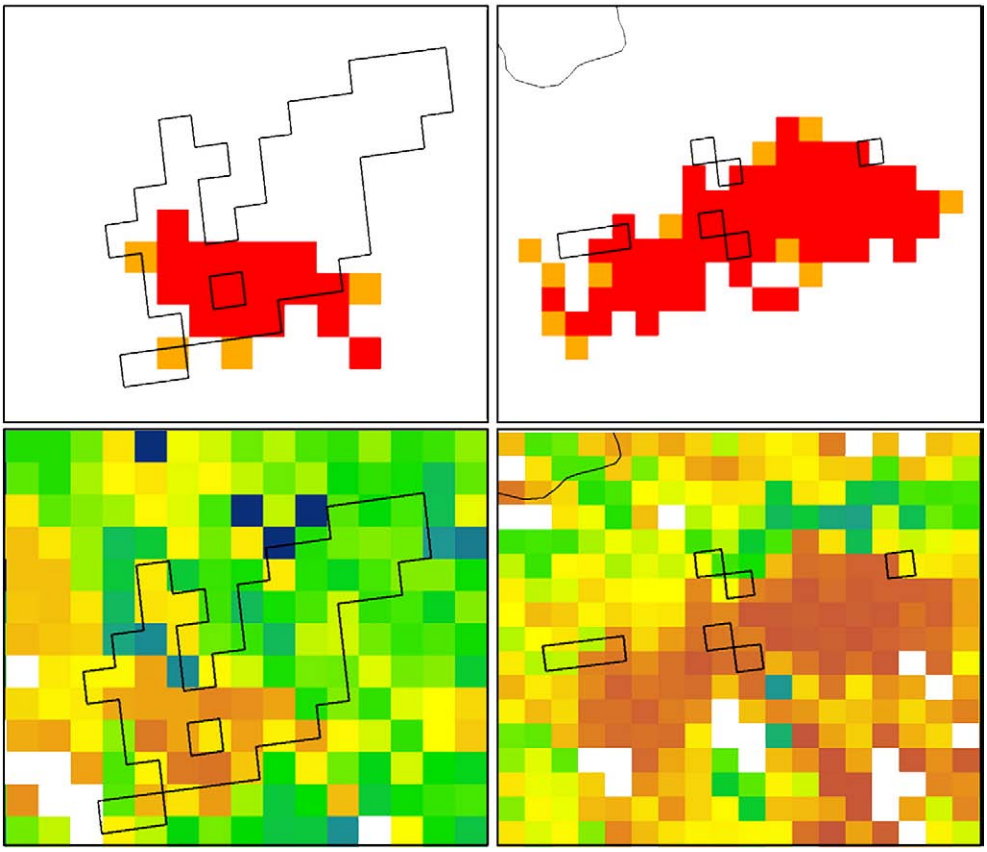

Fig. 7. Top panel shows that the 2006 MGDI results show differences with the validation data (black polygons). The 2006 EVI data (bottom panel) shows decreases mapped in brown (large decrease) and yellow (small decrease) that correspond to the MGDI results.

pre-Katrina (2005) Landsat image of the area including the Bayou Sauvage NWR shows deep vibrant green vegetation (Fig. 10d). Post-Katrina (2006) the vegetation turned to bright red signifying mortality (Fig. 10e). The sudden vegetation mortality is detected by the MGDI. Note the narrow strip of green vegetation north of the Wildlife Refuge and extending along the shoreline in the 2006 Landsat image (Fig. 10e). The MGDI results are in agreement, detecting only two moderate severity pixels along the shoreline. This is a good example of the sensitivity of the MGDI to high severity impacts to vegetation at a relatively small scale.

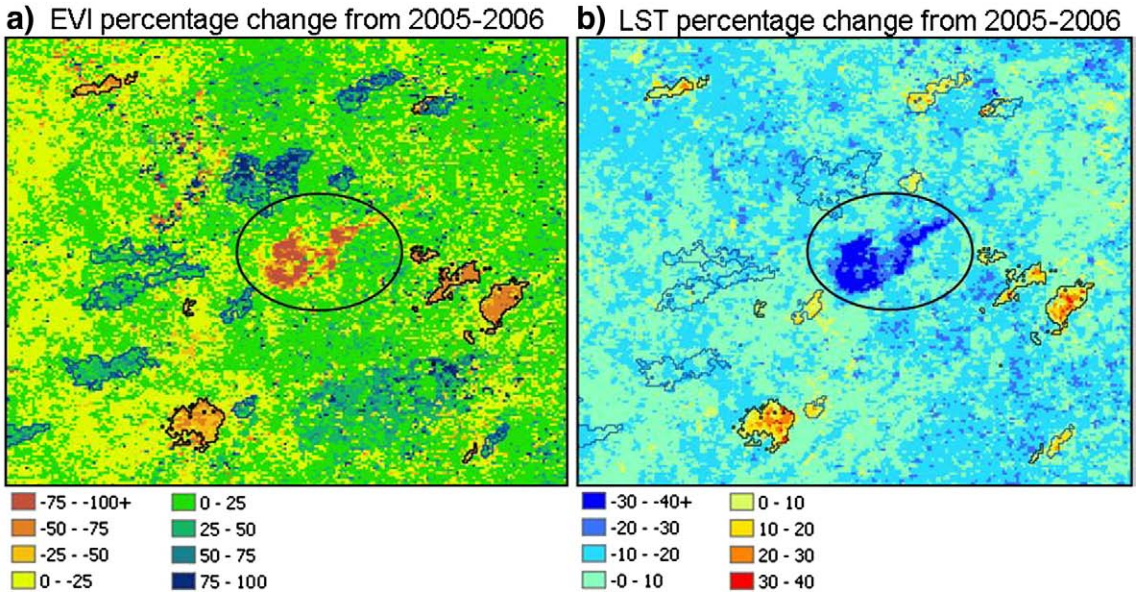

Fig. 8. A non-fire disturbance (circle outline) detected by the MGDI in Quebec Province in 2006 shows a sharp reduction in $EVI_{max\ post}$ from 2005 to 2006 similar to the 2006 wildfire perimeter maps (black outlines). 2005 wildfire perimeters (blue) show a positive EVI change due to vegetation recovery (a). However, the maximum LST decreased by more than 30% from 2005 to 2006, opposite of areas burned by wildfire in 2006 (b). Flood induced vegetation mortality resulting in increased partitioning of incoming solar radiation to latent heat flux is the likely cause of this disturbance.

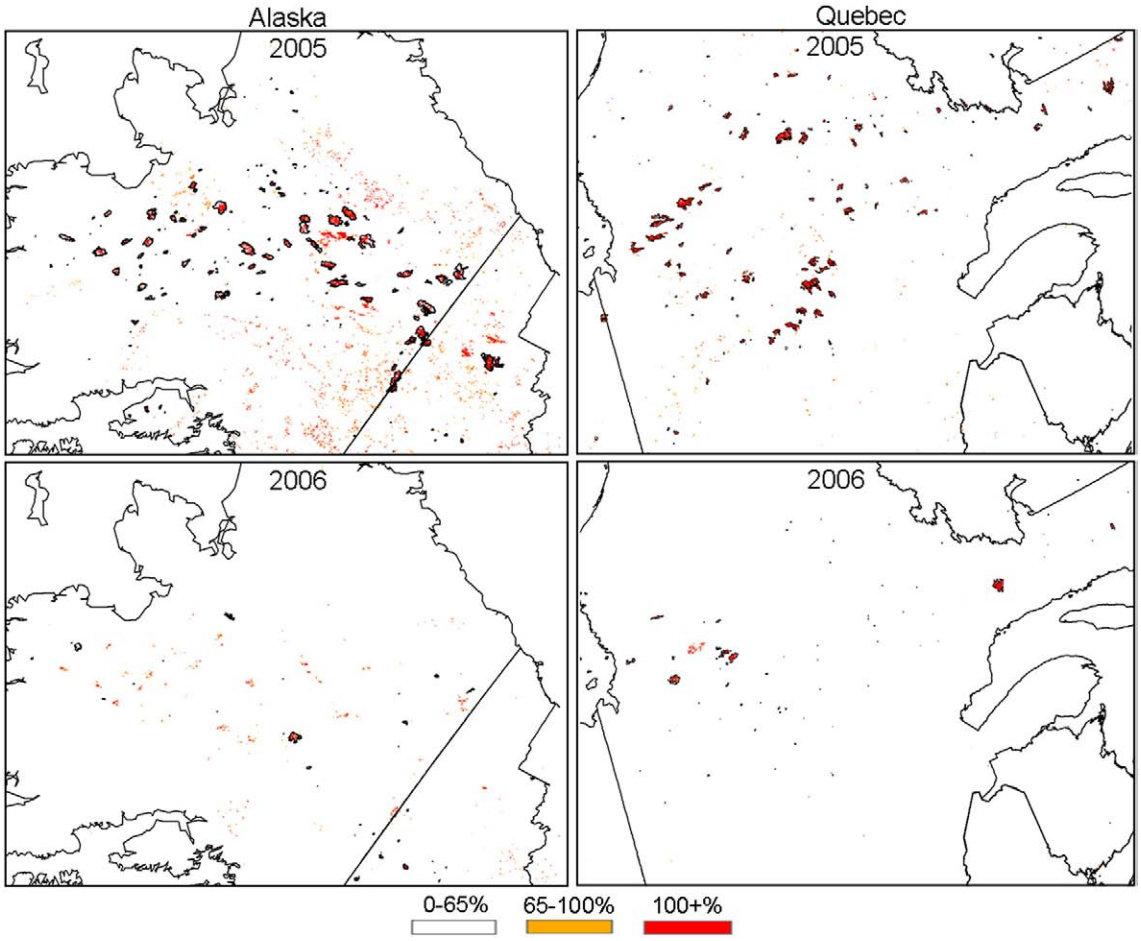

Fig. 9. Regional images of the 2005 and 2006 MGDI results in Alaska, USA and Quebec, Canada illustrate high interannual variability in area burned.

Hurricane Rita made landfall on September 24th, 2005 near the Texas/Louisiana border (Fig. 11a). The 2006 MGDI detected large patches of severe and moderate intensity disturbance concentrated along the shoreline in the windfall area (Fig. 11b). Compared to the results of Hurricane Katrina's windfall area, there is more high severity disturbance near the shoreline and less moderate severity disturbance inland. Hurricane Wilma made landfall on Mexico's Yucatan Peninsula on Oct. 19th, 2005 several weeks after Katrina and Rita's landfall. The stormtrack (Fig. 11c) illustrates that Wilma hit the tip of the Yucatan Peninsula before recurving east and losing strength. The 2006 MGDI flagged pixels in a patchy mosaic of mostly moderate severity disturbance concentrated at the tip of the Yucatan Peninsula where Hurricane Wilma made landfall (Fig. 11d).

7.3. Deforestation and logging detection

We examine the 2006 MGDI results for detection of deforestation and logging across a scene in British Columbia. Deforested pixels are expected to have a low EVI value (yellow or brown color) relative to the surrounding undisturbed vegetation (green or blue color). All non-woody pixels (e.g. croplands) are masked out in white (Fig. 12a). The remaining pixels constitute the woody vegetation in the area classified by MODIS land cover. The 2006 MGDI results are overlayed on the $EVI_{max\ post}$ data and include a large wildfire in the lower left of the image. On the forest–agricultural interface the MGDI flags relatively small groups of pixels with a variety of patch size and severity. Closer examination of a small, high severity disturbance in 2006 (Fig. 12b) reveals that the $EVI_{max\ post}$ is lower for the pixels flagged as disturbed than for the surrounding pixels (Fig. 12c). Pointers inserted into Google Earth that correspond to the center of the pixels flagged by the MGDI overlap a large clear-cut area (Fig. 12d). Note that the other clear-cuts visible in the Google Earth image are of significantly smaller size. Fig. 12e shows an area flagged as disturbed by the 2006 MGDI that is directly on the forest–agriculture interface. The disturbed pixels have the lowest $EVI_{max\ post}$ values of any pixels in the area (Fig. 12f). The pixel pointers inserted into the Google Earth image illustrate the complexity of disturbance detection along the shifting mosaic boundary of the forest–agricultural interface (Fig. 12g). Thin densely arranged clear-cuts adjoin agricultural areas suggesting that a given MODIS pixel could include a mixture of forest and agriculture areas.

8. Continental statistics

For the woody ecosystems of North America the MGDI estimates total disturbance rates of 1.5% during 2005 and 0.5% during 2006 (Table 2). This translates to a total surface area of 195,580 km^2 of LSED in 2005 and 67,451 km^2 in 2006. This large interannual variability is illustrated by regional images dominated by wildfire in 2005 and with much fewer wildfires in 2006 (Fig. 9). For forests, shrublands, and savannas the percentage of disturbed pixels was nearly threefold or more in 2005 than 2006 (Table 2). Area disturbed for major woody biome groups is given in square kilometers in Table 2. Shrublands had the largest area impacted by LSED during 2005 and 2006, followed by forests, and savannas. The NAFD study has estimated disturbance rates of 1–1.5% of forest cover per year during the 80's and 90's across the U.S. (Goward et al., 2008). The NAFD study is based on a sampling of scattered sites across the U.S. as opposed to continuous coverage.

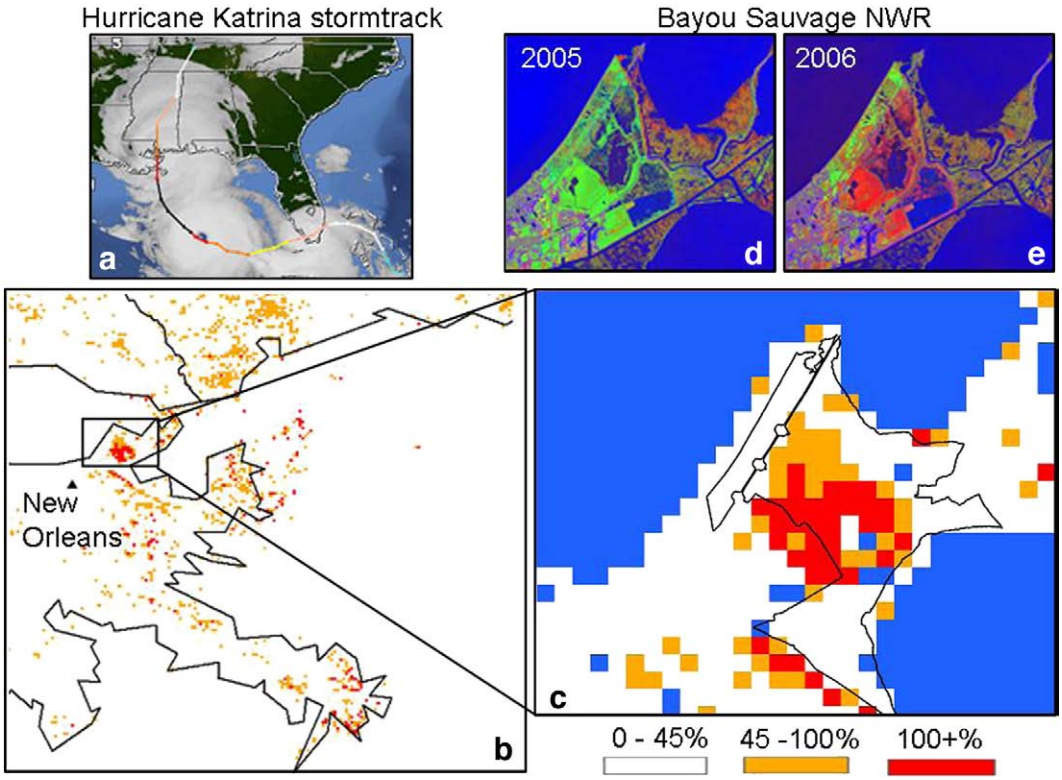

Fig. 10. Hurricane detection results showing a comparison between the stormtrack of Hurricane Katrina (a) and the 2006 MGDI results (b). Zoom-in of the Bayou Sauvage NWR (black poloygon) with water mapped in blue (c) illustrates the association between a large patch of high and moderate severity disturbance and impacts to the Bayou Savage NWR shown in the Landsat images (Credit: USGS) before (d) and after (e) Hurricane Katrina.

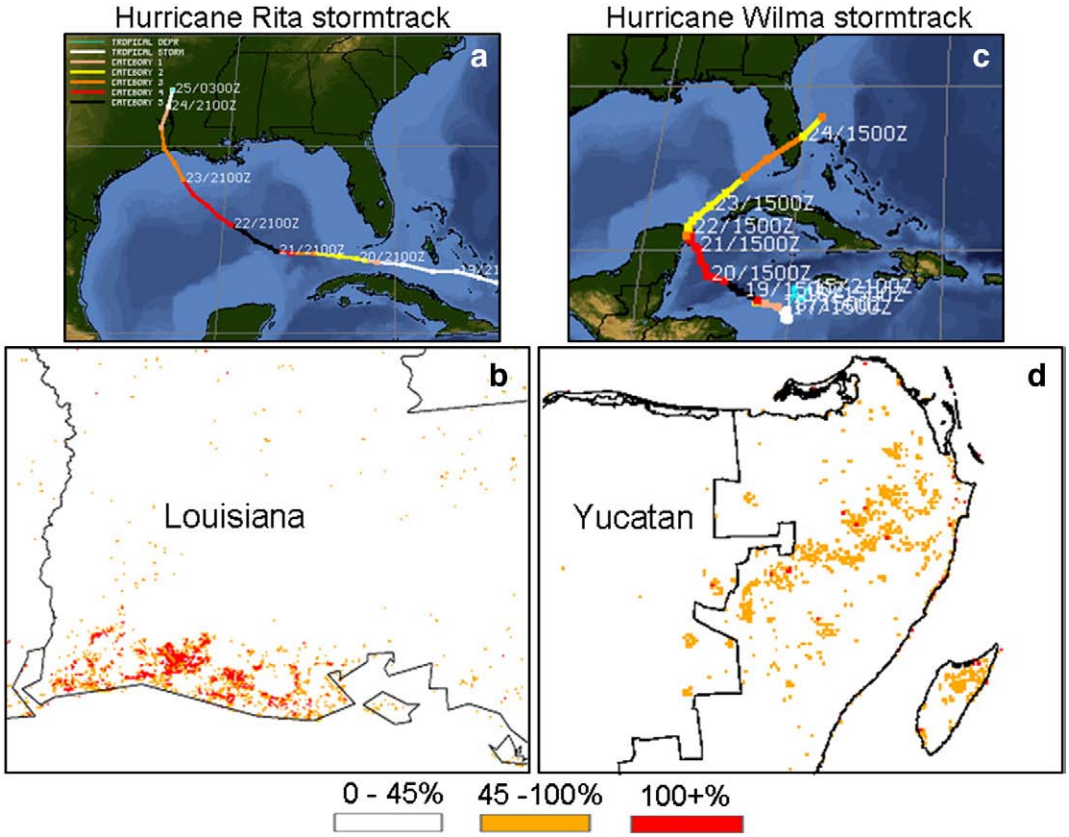

Fig. 11. Hurricane detection results showing a comparison between the stormtrack of Hurricane Rita (a) and HurricaneWilma (c) and the 2006 MGDI results. The MGDI detects large patches of intense disturbance that dominate the coastal area where Hurricane Rita made landfall (b). Hurricane Wilma resulted in widespread, scattered, moderate intensity disturbance (d).

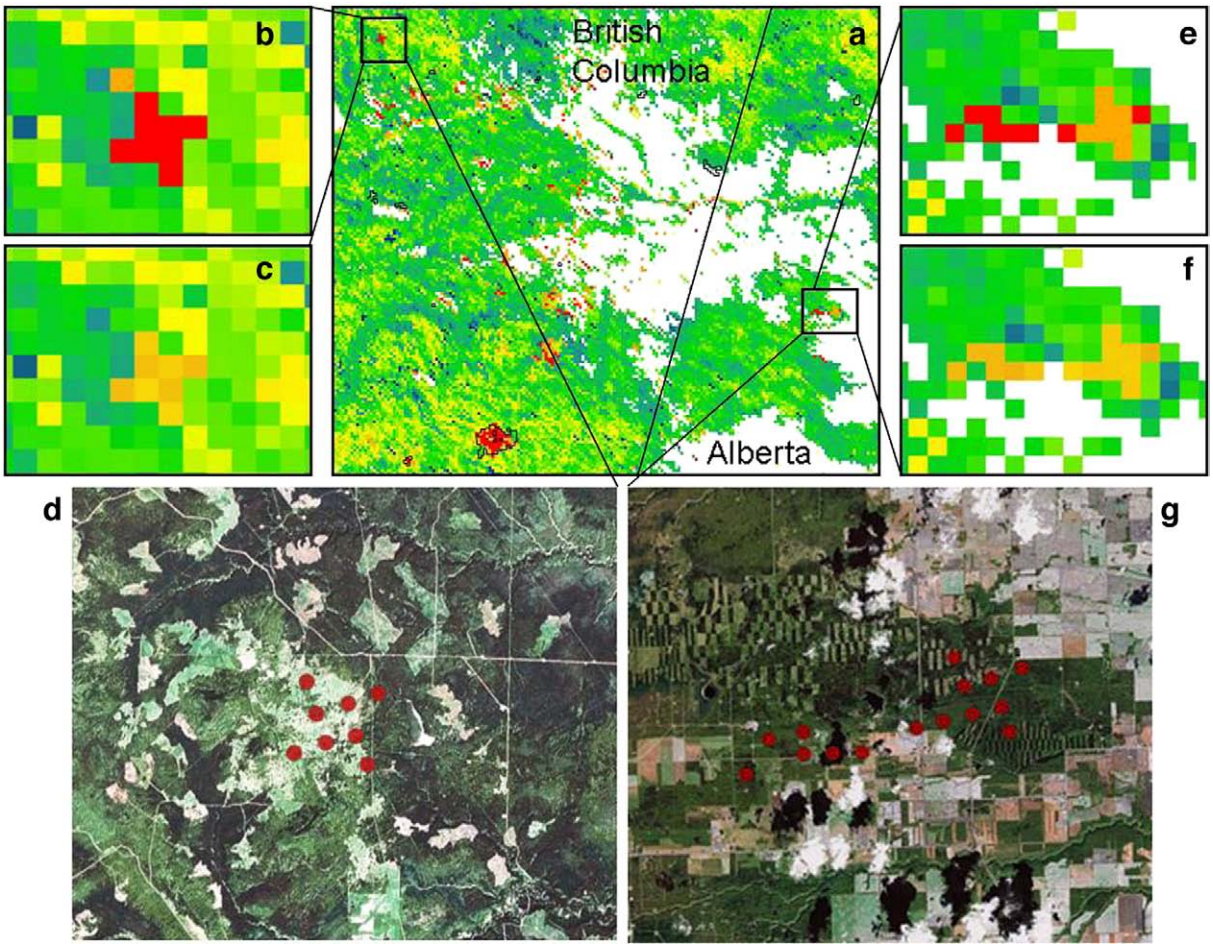

Fig. 12. Deforestation detection along the forest/agricultural interface (colored areas are woody vegetation, white areas are agricultural) in Canada (a). The color palette ranges from blue (very dense vegetation) to green (dense vegetation) to yellow (sparse vegetation) to brown (barren). Pixels flagged with high intensity disturbance (red) by the MGDI (b, e) correspond with a sharp reduction in the $EVI_{max\ post}$ (c, f). Pointers inserted into Google Earth correspond to a large clear-cut area (d) and to a forested area on the border of agriculture where densely placed clear-cuts are visible (g).

The continuous coverage of the MGDI detects disturbance across 1.1% of North America's forests during 2005 and 0.4% during 2006.

9. Discussion

We have demonstrated through a rigorous analysis with burned area datasets from numerous sources and at a variety of spatial scales that the MGDI is capable of accurately detecting the location and extent of wildfire in woody ecosystems while significant improvements have been made to remove background noise. The very strong relationship (2005: $R^2 = 0.91$; 2006: $R^2 = 0.96$) between the MGDI results and the validation data for wildfire across Canada illustrates that with the exception of small wildfires that account for an insignificant percentage of the total burned area, the MGDI is accurately estimating the total burned area.

Few attempts have been made to map the impacts of hurricanes either with field-based measurements or using remotely sensed data. This lack of spatial information makes verification of remotely sensed data difficult. However, the correspondence between pixels flagged high severity and the windfall area of three major hurricanes during 2005 is compelling evidence that the MGDI can detect the location and extent of the most severe impacts from hurricanes. More analyses are needed on the detection of moderate severity impacts throughout the inland windfall area. The comparison between the pre- and post-Katrina Landsat images of the Bayou Sauvage NWR and the 2006 MGDI indicates that the MGDI is accurately detecting relatively small patches of high severity disturbance. When summed across continental scales, these relatively small patches are important to include in estimates of total surface area impacted by LSEDs.

Small-scale logging can be difficult to detect with coarse-resolution data (Potter et al., 2007). Based on the 1-km MODIS pixel size, results here indicate that the MGDI is capable of detecting large or very densely placed logging units and potentially forest clearing on the forest–agricultural interface. These examples highlight the trade-off between resolution of the data and the ability to detect relatively fine-scale land-use changes. We present these results with caution because while the forest–agricultural ecotone is an at-risk area for deforestation, extra care is needed in this area because shifting cultivation results in a mosaic of clearing and fallow that change over time. Such clearings, if identified as new deforestation in a monitoring system,

Table 2
Total area of woody ecosystems in North America, the percent disturbed, and the area disturbed during 2005 and 2006 detected by MGDI instantaneous algorithm.

Biome group	Total area		Percent disturbed (%)		Area disturbed (km^2)	
	% of study area	km^2	2005	2006	2005	2006
Forest	27.5	5,888,595	1.1	0.4	62,749	23,040
Shrub	27.7	5,927,102	1.6	0.6	94,537	36,555
Savanna	7.6	1,625,051	2.4	0.5	38,294	7856
Total/grand mean[a]	62.7	13,440,748	1.5[a]	0.5[a]	195,580	67,451

[a] Grand mean is computed as the total number of disturbed woody pixels divided by the total number of woody pixels.

would falsely inflate deforestation rates in the long term (DeFries et al., 2007). There is the potential that the MODIS land cover is misclassifying some pixels dominated by agriculture as forest. If pixels in agricultural areas are classified as woody vegetation, once clearing occurs the reduction in vegetation density will result in a large MGDI signal and potential false positives. We emphasize that the MGDI is for large-scale regular disturbance mapping and not intended to differentiate small disturbances at the individual pixel level.

The large interannual variability in total disturbed area between 2005 and 2006 indicates that the MGDI algorithm is sensitive to the extreme climatic conditions of 2005. 2005 was one of the hottest years on record in North America and these widespread extreme conditions contributed to increased wildfire and the larger fraction of disturbed woody ecosystems in 2005. It is important to recognize that the MGDI methodology does not focus on any one type of disturbance, but rather detects any disturbance that results in a sustained disruption of a given pixels MGDI value.

The MGDI is now based on 5 years of data, strengthening the computation of natural variability at each pixel. While background noise has been drastically reduced through algorithm improvements, areas remain where the MGDI flags disturbances that could not be verified and are potential false detects. One such area is on the border of the Yukon and the Northwest Territories of Canada. This area has extreme mountainous topography with steep slopes and various aspects. The $EVI_{max\ post}$ values show high spatial variation between neighboring pixels and the interannual variability is very high indicating that there may be problems with the topographic effect (Matsushita et al., 2007). Unreasonable fluctuations in the EVI values can feedback to signal disturbance in the MGDI. Combined, open shrublands and savannas occupy a large part of the study area and are defined by MODIS land cover as having between 10%–60% and 10%–30% woody vegetation cover respectively (Strahler et al., 1999). Annual herbaceous vegetation can be preponderant in these areas and fluctuations in annual herbaceous cover alone could be triggering the MGDI in some open shrublands and savannas. However, the increase in disturbance detected in open shrublands and savannas in 2005 relative to 2006 was equivalent to the increase detected in forests and verified wildfire detection in shrubland and savanna ecosystems is common and therefore important to include in our continental results.

Additional research needs to be done on the ability of the MGDI to accurately detect disturbance due to insect infestation. Bark beetles are ubiquitous in the conifer forests of North America, affecting 47 million ha of nearly every region and coniferous forest type in the last 10 years (Raffa et al., 2008). Clearly not all of this activity results in a sustained disruption of ecosystem structure and function. Raffa (2008) describes various internal and external controls that exert influence and feedbacks on the population dynamics of bark beetles, essentially keeping most beetle activity well within the range of natural variability. Once critical thresholds have been breached and population eruption occurs at the landscape scale, then the infestation begins to have impacts that meet the definition of a LSED. Still, even population eruptions may only result in 60% tree mortality (Raffa et al., 2008) leaving the younger trees, and understory intact. These impacts are subtler than the impacts from wildfire and hurricane. With additional years of data the MGDI will continue to refine the range of natural variability and better distinguish more subtle disturbances from the backdrop of natural variability.

10. Conclusions

The MGDI is developed to serve as an efficient, powerful, automated algorithm for global application that utilizes the strengths of the MODIS LST in combination with the MODIS EVI data. The MDGI is based on universal principles that can be generalized globally for systematic disturbance detection: (1) that vegetation, when left undisturbed, will achieve maximum coverage for a specific environment and (2) that disturbance of vegetation will result in a significantly different surface coverage and a commensurate change in the maximum surface temperature. The basic relationship between LST and vegetation density that the MGDI is based upon is easily understandable and a major advantage over more complex approaches to disturbance detection. We know of no other methodology that uses annual maximum compositing of LST in combination with a spectral VI to detect disturbance. The advantage of automated, continuous coverage of disturbance detection is illustrated by the accurate spatial information on disturbance location and extent combined with continental statistics that are within the range of expected values and capture interannual variability. We anticipate global application of the 1-km MGDI.

Acknowledgments

This project would not have been possible without the financial support from the National Aeronautics and Space Administration (NASA) Earth Observing System (EOS) Natural Resource/Education Training Center (Grant Number NAG 5-12540). We thank Dr. Chambers for helpful discussions on Hurricane Katrina and the University of Wisconsin/CIMSS/SSEC for the use of stormtrack images. The authors are grateful to the CCRS, the USGS, and the USFS for providing wildfire perimeter data.

Appendix A. Supplementary data

Supplementary data associated with this article can be found, in the online version, at doi:10.1016/j.rse.2009.05.016.

References

Amiro, B. D., Todd, J. B., Wotton, B. M., Logan, K. A., Flannigan, M. D., Stocks, B. J., et al. (2001). Direct carbon emissions from Canadian forest fires, 1959–1999. *Canadian Journal of Forest Research*, *31*, 512—525.

Baker, W. L. (1995). Longterm response of disturbance landscapes to human intervention and global change. *Landscape Ecology*, *10*, 143—159.

Bonan, G. B. (2008). Forests and climate change: Forcings, feedbacks, and the climate benefits of forests. *Science*, *320*, 1444—14449.

Borak, J. S., Lambin, E. F., & Strahler, A. H. (2000). The use of temporal metrics for land cover change detection at coarse spatial scales. *International Journal of Remote Sensing*, *21*, 1415—1432.

Canadell, J. G., Mooney, H. A., Baldocchi, D. D., Berry, J. A., Ehleringer, J. R., Field, C. B., et al. (2000). Carbon metabolism of the terrestrial biosphere: A multi-technique approach for improving understanding. *Ecosystems*, *3*, 115—130.

Carlson, T. N., Boland, F. E., Dodd, J. K., & Benjamin, S. G. (1981). Satellite estimation of the surface energy balance, moisture availability and thermal intertia. *Journal of Applied Meteorology*, *20*, 67—87.

Chambers, J. Q., Fisher, I. F., Zeng, H., Chapman, E. L., Baker, D. B., & Hurtt, G. C. (2007). Hurricane Katrina's carbon footprint on U.S. Gulf Coast forests. *Science*, *318*.

Dale, V. H., Joyce, L. A., McNulty, S., Neilson, R. P., Ayres, M. P., Flannigan, M. D., et al. (2001). Climate change and forest disturbances. *BioScience*, *51*, 723—734.

DeFries, R., Achard, F., Brown, S., Herold, M., Murdiyarso, D., Schlamadinger, B., et al. (2007). Earth observations for estimating greenhouse gas emissions from deforestation in developing countries. *Environmental Science and Policy*, *10*, 385—394.

Duro, D. C., Coops, N. C., Wulder, M. A., & Han, T. (2007). Development of a large area biodiversity monitoring system driven by remote sensing. *Progress in Physical Geography*, *31*, 235—260.

Emanuel, K. (2005). Increasing destructiveness of tropical cyclones over the past 30 years. *Nature*, *436*, 686—688.

Flannigan, M. D., Stocks, B. J., & Wotton, B. M. (2000). Climate change and forest fires. *The Science of the Total Environment*, *262*, 221—229.

Fraser, R. H., Li, Z., & Cihlar, J. (2000). Hotspot and NDVI Differencing Synergy (HANDS): A new technique for burned area mapping over boreal forest. *Remote Sensing of Environment*, *74*, 362—376.

Friedl, M. A., & Davis, F. W. (1994). Sources of variation in radiometric surface temperature over a tallgrass prairie. *Remote Sensing of Environment*, *48*, 1—17.

Goetz, S. J. (1997). Multi-sensor analysis of NDVI, surface temperature and biophysical variables at a mixed grassland site. *International Journal of Remote Sensing*, *18*, 71—94.

Goward, S. N., Cruickshanks, G. D., & Hope, A. S. (1985). Observed relation between thermal emission and reflected spectral radiance of a complex vegetated landscape. *Remote Sensing of Environment*, *18*, 137—146.

Goward, S. N., & Hope, A. S. (1989). Evapotranspiration from combined reflected solar and emitted terrestrial radiation: Preliminary FIFE results from AVHRR data. *Advanced Space Research*, *9*, 239−249.

Goward, S. N., Masek, J. G., Cohen, W., Moisen, G., Collatz, G. J., Healey, S., et al. (2008). Forest disturbance and North American carbon flux. *EOS, Transactions*, *89*, 105−116.

Grier, C. G., & Running, S. W. (1977). Leaf area of mature northwestern coniferous forests: Relation to site water balance. *Ecology*, *58*, 893−899.

Gurney, R., & Camillo, P. J. (1984). Modeling daily evapotranspiration using remotely sensed data. *Journal of Hydrology*, *69*, 305−324.

Hayasaka, H., Nakau, K., Kushida, K., Fukuda, M., & Jandt, R. (2006). Recent increases in large wildfires in the boreal forest of Alaska in relation to weather patterns. *Forest Ecology and Management*, *234*, S106.

Huete, A., Didan, K., Miura, T., Rodriguez, E. P., Gao, X., & Ferreira, L. G. (2002). Overview of the radiometric and biophysical performance of the MODIS vegetation indices. *Remote Sensing of Environment*, *83*, 195−213.

Huete, A., Justice, C., & Leeuwen, W. v. (1999). *MODIS Vegetation Index (MOD 13) Algorithm Theoretical Basis Document* (http://modis.gsfc.nasa.gov/data/atbd/atbd_mod13.pdf)

Huxman, T. E., Smith, M. D., Fay, P. A., Knapp, A. K., Shaw, M. R., Loik, M. E., et al. (2004). Convergence across biomes to a common rain-use efficiency. *Nature*, *429*, 651−654.

Knapp, A. K., & Smith, M. D. (2001). Variation among biomes in temporal dynamics of aboveground primary production. *Science*, *291*, 481−484.

Kurz, W. A., Stinson, G., Rampley, G. J., Dymond, C. C., & Neilson, E. T. (2008). Risk of natural disturbances makes future contribution of Canada's forests to the global carbon cycle highly uncertain. *Proceedings of the National Academy of Sciences of the United States of America*, *105*, 1551−1555.

Lambin, E. F., & Ehrlich, D. (1995). Combining vegetation indices and surface temperature for land-cover mapping at broad spatial scales. *International Journal of Remote Sensing*, *16*, 573−579.

Lambin, E. F., & Ehrlich, D. (1996). The surface temperature–vegetation index space for land cover and land-cover change analysis. *International Journal of Remote Sensing*, *17*, 463−487.

Lambin, E. F., & Strahler, A. H. (1994). Indicators of land-cover change for change-vector analysis in multitemporal space at coarse spatial scales. *International Journal of Remote Sensing*, *15*, 2099−2119.

Lugo, A. E. (2000). Effects and outcomes of Caribbean hurricanes in a climate change scenario. *The Science of the Total Environment*, *262*, 243−251.

Lugo, A. E., & Scatena, F. N. (1996). Background and catastrophic tree mortality in tropical moist, wet, and rain forests. *Biotropica*, *28*, 585−599.

Mannstein, H. (1987). Surface energy budget, surface temperature and thermal intertia, in Remote Sensing Applications in Meteorology and Climatology. In R. A. Vaughan & D. Reidel (Eds.), Dordrecht, Netherlands: A Reidel Publishing Co.

Matsushita, B., Yang, W., Chen, J., Onda, Y., & Qiu, G. (2007). Sensitivity of the Enhanced Vegetation Index (EVI) and Normalized Difference Vegetation Index (NDVI) to topographic effects: A case study in high-density cypress forest. *Sensors*, *7*, 2636−2651.

Mildrexler, D. J., Zhao, M., Heinsch, F. A., & Running, S. W. (2007). A new satellite-based methodology for continental scale disturbance detection. *Ecological Applications*, *17*, 235−250.

Mildrexler, D. J., Zhao, M., & Running, S. W. (2006). Where are the hottest spots on Earth? *EOS, Transactions*, *87*, 461, 467.

Nelson, R., & Holben, B. (1986). Identifying deforestation in Brazil using multi-resolution satellite data. *International Journal of Remote Sensing*, *7*, 429−448.

Nemani, R. R., Pierce, L. L., & Running, S. W. (1993). Developing satellite derived estimates of surface moisture status. *Journal of Applied Meteorology*, *32*, 548−557.

Nemani, R. R., & Running, S. W. (1989). Estimation of regional surface resistance to evapotranspiration from NDVI and Thermal-IR AVHRR data. *Journal of Applied Meteorology*, *28*, 276−284.

Nemani, R. R., & Running, S. W. (1997). Land cover characterization using multitemporal red, near-IR, and thermal-IR data from NOAA/AVHRR. *Ecological Applications*, *7*, 79−90.

Nemani, R. R., Running, S. W., Pielke, R. A., & Chase, T. N. (1996). Global vegetation changes from coarse resolution satellite data. *Journal of Geophysical Research*, *101*, 7157−7162.

Picket, S. T. A., Collins, S. C., & Armesto, J. J. (1987). Models, mechanisms, and pathways of succession. *Botanical Review*, *53*, 335−371.

Picket, S. T. A., & White, P. S. (1985). *The Ecology of Natural Disturbance as Patch Dynamics*. New York: Academic Press.

Potter, C., Kumar, V., Klooster, S., & Nemani, R. R. (2007). Recent history of trends in vegetation greenness and large-scale ecosystem disturbances in Eurasia. *Tellus*, *59*, 260−272.

Potter, C., Tan, P. N., Kumar, V., Kucharik, C., Klooster, S., Genovese, V., et al. (2005). Recent history of large-scale ecosystem disturbances in North America derived from the AVHRR satellite record. *Ecosystems*, *8*, 808−824.

Potter, C., Tan, P., Steinback, M., Klooster, S., Kumar, V., Myneni, R., et al. (2003). Major disturbance events in terrestrial ecosystems detected using global satellite data sets. *Global Change Biology*, *9*, 1005−1021.

Price, J. C. (1990). Using the spatial context in satellite data to infer regional scale evapotranspiration. *IEEE Transactions on Geoscience and Remote Sensing*, *28*, 940−948.

Raffa, K. F., Aukema, B. H., Bentz, B. J., Carroll, A. L., Hicke, J. A., Turner, M. G., et al. (2008). Cross-scale drivers of natural disturbances prone to anthropogenic amplification: The dynamics of bark beetle eruptions. *BioScience*, *58*, 501−517.

Reice, S. R. (1994). Nonequilibrium determinants of biological community structure. *American Naturalist*, *82*, 424−435.

Roy, D. P., Kennedy, P., & Folving, S. (1997). Combination of the Normalized Difference Vegetation Index and surface temperature for regional scale European Forest cover mapping using AVHRR data. *International Journal of Remote Sensing*, *18*, 1189−1195.

Running, S. W. (2006). Is global warming causing more, larger wildfires? *Science*, *313*, 927−928.

Running, S. W. (2008). Ecosystem disturbance, carbon, and climate. *Science*, *321*, 652−653.

Sellers, P. J., Hall, F. G., Asrar, G., Strebel, D. E., & Murphy, R. E. (1988). The first ISLSCP Field Experiment (FIFE). *Bulletin of the American Meteorological Society*, *69*, 22−27.

Sequin, B., & Itier, B. (1983). Using midday surface temperature to estimate daily evaporation from satellite thermal IR data. *International Journal of Remote Sensing*, *4*, 371−383.

Smith, R. C. G., & Choudhury, B. J. (1991). Analysis of normalized difference and surface temperature observations over southeastern Australia. *International Journal of Remote Sensing*, *12*, 2021−2044.

Sousa, W. P. (1984). The role of disturbance in natural communities. *Annual Review of Ecology and Systematics*, *15*, 353−391.

Stocks, B. J., Fosberg, M. A., Lynham, T. J., Mearns, L., Wotton, B. M., Yang, Q., et al. (1998). Climate change and forest fire potential in Russian and Canadian boreal forests. *Climatic Change*, *38*, 1−13.

Strahler, A., Muchoney, D., Borak, J., Friedl, M., Gopal, S., Lambin, E., et al. (1999). *MODIS Land Cover Product Algorithm Theoretical Basis Document (ATBD) version 5.0* (http://modis.gsfc.nasa.gov/data/atbd/atbd_mod12.pdf)

Tilman, D. (1985). The resource-ratio hypothesis of plant succession. *American Naturalist*, *125*, 827−852.

Turner, M. G., Dale, V. H., & Everham, E. E., III (1997). Fires, hurricanes, and volcanoes: Comparing large-scale disturbances. *Bioscience*, *47*, 758−768.

van der Werf, G. R., Randerson, J. T., Collatz, G. J., Giglio, L., Kasibhatla, P. S., Arellano, A. F., Jr., et al. (2004). Continental-scale partitioning of fire emissions during the 1997 to 2001 El Niño/La Niña period. *Science*, *303*, 73−76.

Wan, Z., Zhang, Y., Zhang, Q., & Li, Z. L. (2004). Quality assessment and validation of the MODIS global land surface temperature. *International Journal of Remote Sensing*, *25*, 261−274.

Waring, R. H., & Running, S. W. (2007). *Forest ecosystems: Analysis at multiple scales*, 3rd ed. San Diego, CA: Elsevier Academic Press.

Westerling, A. L., Hidalgo, H. G., Cayan, D. R., & Swetnam, T. W. (2006). Warming and earlier spring increase Western U.S. forest wildfire activity. *Science*, *313*.

White, A. B., Praveen, K., & Tcheng, D. (2005). A data mining approach for understanding topographic control on climate-induced inter-annual vegetation variability over the United States. *Remote Sensing of Environment*, *98*, 1−20.

Wiedinmyer, C., & Neff, J. C. (2007). Estimates of CO_2 from fires in the United States: Implications for carbon management. *Carbon Balance and Management*, *2*, 1−33.